IOP Publishing Smart Materials and Structures
Smart Mater. Struct. 27 (2018) 014001 (9pp) https://doi.org/10.1088/1361-665X/aa87da

A flexible electrostatic kinetic energy harvester based on electret films of electrospun nanofibers

Y Lu, M Capo-Chichi, Y Leprince-Wang and P Basset

Université Paris-Est, ESYCOM (EA2552), CNAM, ESIEE Paris, UPEM, Marne-la-Vallée, France

E-mail: p.basset@esiee.fr

Received 25 April 2017, revised 20 August 2017
Accepted for publication 23 August 2017
Published 4 December 2017

Abstract

This paper reports a paper-based electrostatic kinetic energy harvester (e-KEH) implementing multilayered electret films based on electrospun nanofibrous material. It is the first time that a fully flexible electret-based e-KEH is reported. The proposed electret, PVDF-PTFD nanofibrous covered by Parylene C, has a faster stabilization of surface potential than a planar thin film of Parylene C, and a higher stability of charge storage. With a maximum force of 0.5 N and a 3-layer electret, the device capacitance increases from 25 to 100 pF during a pressing operation. Working with the optimal resistive load of 16 MΩ, the device pressed manually delivers a peak instantaneous power up to 45.6 μW and an average energy of 54 nJ/stroke, corresponding to a peak instantaneous power density of 7.3 μW cm^{-2} and an average energy density of 8.6 nJ cm^{-2}/stroke. Within 450 manual strokes, a 10 nF capacitor is charged up to 8.5 V by the prototype through a full-wave diode bridge. On a 1 μF capacitor, the energy delivery of 9.9 nJ/stroke has been obtained with a 10 Hz pressing movement excited by a vibrator with a maximum force of 0.5 N.

Keywords: kinetic energy harvesting, flexible system, electrospinning, electret, AC–DC rectifying

(Some figures may appear in colour only in the online journal)

1. Introduction

Kinetic energy harvesters (KEHs) are aimed at converting the kinetic energy extensively existing in the environment into electric energy, so as to supply power to portable or distributed electronics instead of batteries. Thanks to the rich source of ambient energy, the devices will not run out of power as batteries, nor is any replacement needed. Flexible KEHs are reported in recent years, including piezoelectric [1, 2] and triboelectric KEHs [3, 4], which are applicable for wearable electronics or for installation on complex surfaces. The reported flexible KEHs work mostly in a contact-driven deformation mode. According to the literature, the typical energy conversion density of the piezoelectric KEHs is 0.1–1 μJ cm^{-2} per cycle [5, 6], while the triboelectric KEHs offer peak instantaneous power of ~10 μW cm^{-2} under the pressure of 30 mN cm^{-2} [3]. However, the efficiency of these KEHs is very low considering the large pressure applied during the operation. It is thus desirable to improve their efficiency through systematic optimization.

Electrostatic KEHs can be modelled as a variable capacitor biased by an internal DC voltage, where the energy delivery during each charge–voltage (QV) cycle is maximized by high internal bias voltage V_{bias} and high ratio of capacitance variation [7]. Electrets are widely used sources to produce internal bias voltages in capacitive KEHs [8], and the stability of storage charge is a cardinal property of electret for its lifetime. As stated in reference [9], the charge stored in an electret are mostly confined within a superficial region with a minuscule thickness, in other words, charge trapping takes place more easily in the surface than the internal region of a material. Thus it is desirable to introduce a rough surface to the electret in order to improve the charge storage stability. Furthermore, the chemical nature of electrets is also critical to

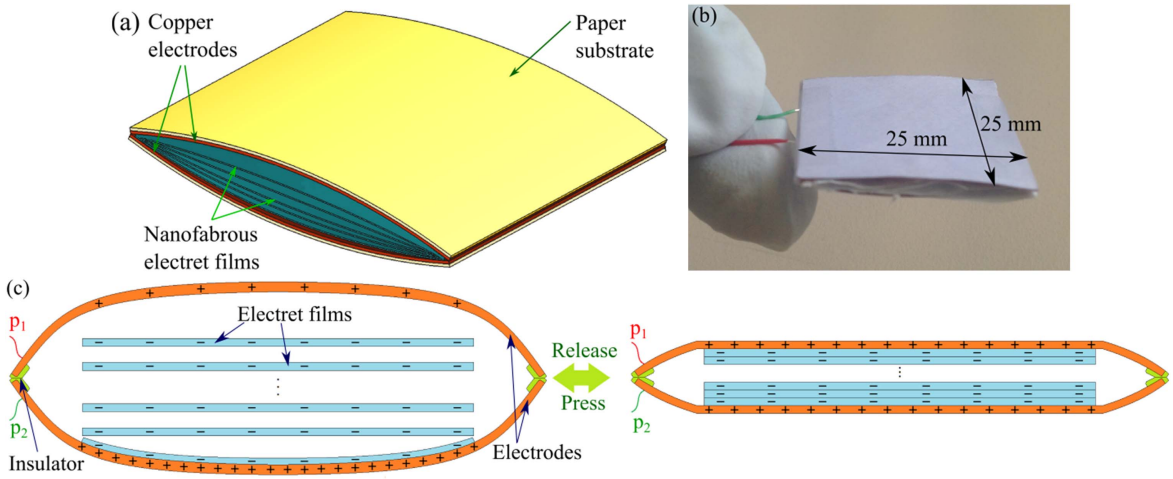

Figure 1. Schematic (a), photograph (b), and working principle (c) of the proposed low-frequency e-KEH.

the charge stability. Firstly the material itself must be a good insulator. In addition, certain functional groups such as Benzene rings and halogen elements can help elongate the lifetime of charge storage in the material [10, 11]. The most commonly applied electret materials include fluoropolymers such as CYTOP [12], and phenyl polymers such as Parylene C [13].

As a mature industrial technique [14], electrospinning is an inexpensive way to fabricate a variety of solvable polymers into fibrous materials with sub-micro or nano-scale dimensions [15], producing high specific surface area films. However, it is difficult to obtain stable charge storage using electrospun nanofibrous materials. Even though solvable polymers such as PET are good electret in bulk volume, the charge storage stability of electrospun nanofibers is poor [16]. Other polymers are not suitable for electrospinning process because of either low solubility (such as Parylene C) or low cure rate (such as CYTOP).

In this work, a first flexible electrostatic KEH is proposed, based on an electret made of electrospun nanofibrous scaffold covered by CVD-deposited Parylene C. The proposed electret has both a large specific area for charge storage and a better storage stability than planar Parylene C films. A high internal bias is provided by a stack of multiple electret films. In section 2, the structure of the device is described and the working principle is presented. The preparation and characterization experiments for the electret material are discussed in section 3. The characterization of the device including the capacitance variation and the power measurements are discussed in section 4.

2. Device description

The device has a sandwich structure with two electrodes on top and on bottom, and stacked electret films in between, as shown in figure 1(a). The 2.5 cm × 2.5 cm square-shaped electrodes are made of coper tapes sticking on paper substrates. The two electrodes are connected mechanically with tape along two parallel edges, and are insulated from each other electrically at the junction edges also by tape. A foam-like stacked electret thin film structure, working as a source of internal bias, is inserted between the two electrodes. Each layer of electret is based on electrospun nanofibrous material and is charged negatively separately beforehand. The photograph of the device is shown in figure 1(b).

The device is operated in a press-and-release mode as shown in figure 1(c). The two electrodes of the device form a gap-closing variable capacitor C_v. By applying a mechanical force on the electrodes, C_v will vary with the change of gap between electrodes: C_{max} is reached after pressing operation and C_{min} after releasing operation. An air gap of 1–2 mm between the top and bottom electrode can be achieved each time the structure is released. Meanwhile, the curved shape of both electrodes can be recovered thanks to the electrodes' stiffness and the sticking to the releasing tap-body. The electric field is generated by each layer of electret film located between the electrodes, and is reinforced by stacking several films. The distribution of the electret is random, and results in an asymmetric electric field with a large probability. The electret films as a whole can be modeled as a bias voltage V_{bias} in series with the transducer variable capacitor C_v. Consequently, certain energy can be delivered within each QV cycle induced by the variation of capacitance C_v [17].

The energy converted by each QV cycle is influenced by the bias voltage and the capacitance, leading to a theoretical optimal KEH configuration. In a rectangular QV cycle as shown in figure 2, the energy converted within one QV cycle is given by the following equation [17]:

$$\Delta E = 2C_{min}V_{bias}^2[(\eta - 1) - (\eta + 1)\eta_v]\eta_v, \quad (1)$$

where C_{min} and C_{max} are the minimum and maximum values of C_v, $\eta = C_{max}/C_{min}$ is the ratio between the maximum and minimum capacitance, $\eta_v = \Delta V/V_{bias}$ is the ratio of voltage variation $\Delta V = V_{max} - V_{min}$ (shown in figure 2) versus the bias voltage. The KEH can be approached as a parallel plate capacitor:

$$C_v = \bar{\varepsilon}a^2/d, \quad (2)$$

where $\bar{\varepsilon}$ is the average dielectric constant of the material

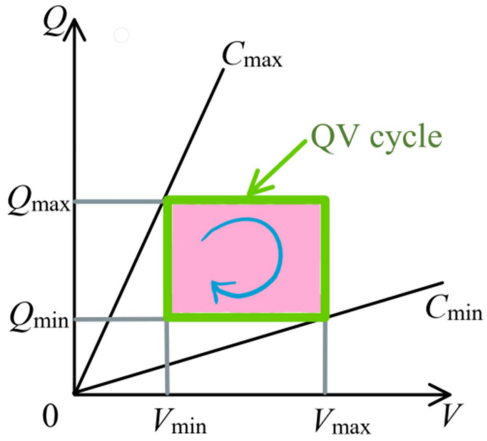

Figure 2. A rectangular QV cycle consisting of 2 constant voltage processes and 2 constant charge processes.

between the electrodes, a is the dimension of the side of the electrodes, d is the distance between the electrodes. Therefore, C_{max} and C_{min} can be deduced:

$$C_{max} = \varepsilon_e a^2/d_{min}; \quad C_{min} = \varepsilon_c a^2/d_{max}, \tag{3}$$

where ε_e is the dielectric constant of the electret films, ε_c is the equivalent dielectric constant of the combined structure of air and electret films. d_{min} and d_{max} are the minimum and maximum distance between electrodes respectively.

Considering the influence of the number of electret layers on V_{bias} and d_{min}:

$$V_{bias} = NV_s \quad d_{min} = Nd_s, \tag{4}$$

where N is the number of electret layers, V_s is the bias voltage offered by a single electret layer, while d_s is the thickness of each electret film. Thus, the influence of N on ΔE is shown as follows:

$$\Delta E = \frac{2\epsilon_c \eta_v a^2 V_s^2}{d_{max}}\left[\frac{\epsilon_e d_{max}}{\epsilon_c d_s}(1-\eta_v) - (1+\eta_v)N\right]N. \tag{5}$$

Thus we can deduce there should be an optimal number of electret films (N_{opt}) that ensures the KEH to offer the maximum output power.

The asymmetric distribution of electric field under the released status is crucial for the proposed KEH: when the KEH is pressed, the amounts of charge on top and bottom electrodes are equal. Thus, only when the charges induced on the two electrodes differ from each other at released status, can any power be transduced by the KEH. That is to say, besides V_{bias} and C_v, the positions of the multi-layers of electret also affect the performance of the KEH. The optimal position for the electrets is to always stick to the same electrode. However, this situation cannot be realized on the basis of the current design, because of the repulsive force between electret layers.

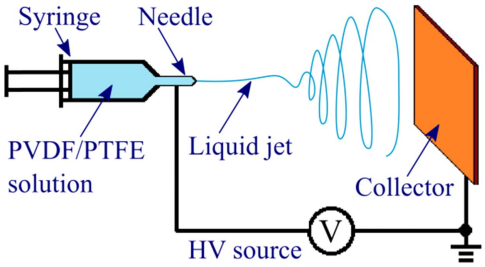

Figure 3. Schematic of electrospinning experimental setup.

3. Material preparation

3.1. Preparation of nanofibrous electret

Firstly a nanofibrous scaffold is prepared through electrospinning method to fabricate a nanostructured basement. The solvent is a mixture of acetone and dimethylformamide, with the volume ratio of 1:1 (weight ratio of 1:1.32) at room temperature, obtained by a magnetic stirring at 60 °C for 30 min. PVDF and PTFE powders are mixed with a weight ratio of 5:1 before being added to the solvent. After a continuous magneto stirring at 60 °C for 24 h, a uniform solution is formed with a solute percentage of mass of 18%.

The PVDF/PTFE solution is then contained in a syringe and subjected to an electrospinning process; the schematic of the experimental setup is shown in figure 3. A syringe pump controls the solution pumping rate. The injection port of the syringe is connected to high voltage, while at a distance of 15 cm from the tip of the syringe port there is a grounded planar electrode, perpendicular to the axis of the syringe and working as a receiver of nanofibrous materials. The high voltage applied is 13 kV, while the liquid is pumped with a rate of 0.7 ml h^{-1} for 2 h. The thickness of nanofibrous film is about 100 μm. The film is then peeled off from the receiver electrode, and cut to desirable shapes by scissors.

Then, the nanofibrous films are put under a Chemical Vapor Deposition (CVD) process to coat an additional layer of Parylene C on their surface. 4 g of Parylene C is deposited in the inlet of the furnace, and this amount corresponds to a 2 μm thick deposition on a planar structure. Figure 4 shows the SEM images of the microstructure of the nanofibrous film before and after Parylene C deposition. We can observe that the real thickness of deposited Parylene C on the fibers is closer to 1 μm rather than 2 μm probably due to the increased specific surface area of the nanostructure in the scaffold. It can also be perceived from the graphs that some tiny nanofibers and small cavities are engulfed by the deposited Parylene C. It can be induced that the more material is deposited, the more nanostructure is covered by the deposited material and disappear, so that the specific surface area is smaller.

3.2. Precharging

Electret films are prepared from 3 different materials through a tri-electrode corona charging process as described in [18]. The high voltage applied on the needle electrode is −12 kV, while the one applied on the grid electrode is −500 V. The

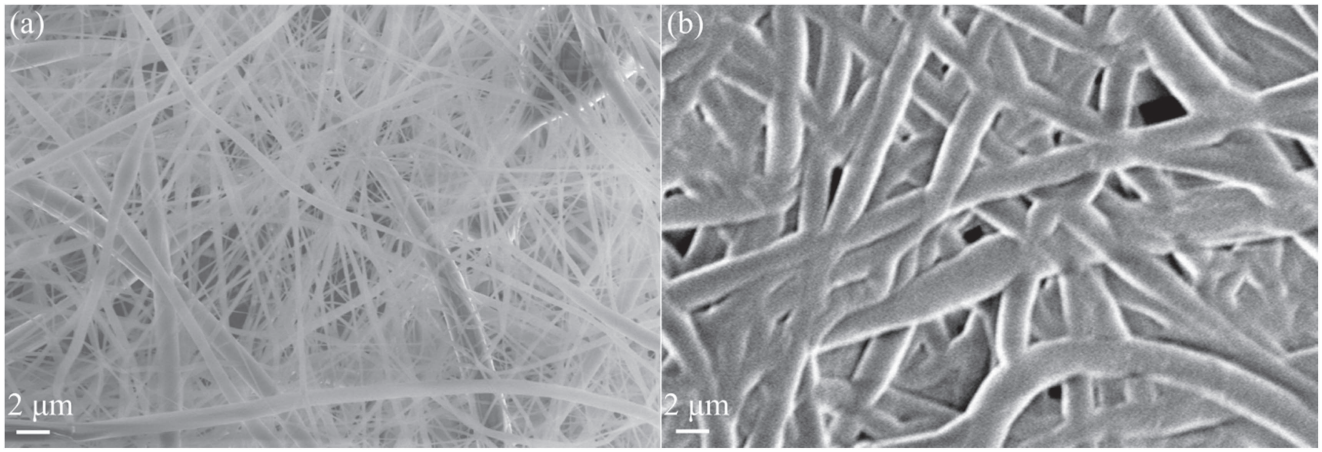

Figure 4. SEM photograph of the electrospun nanofiber of PVDF/PTFE before (a) and after (b) Parylene C deposition by CVD method.

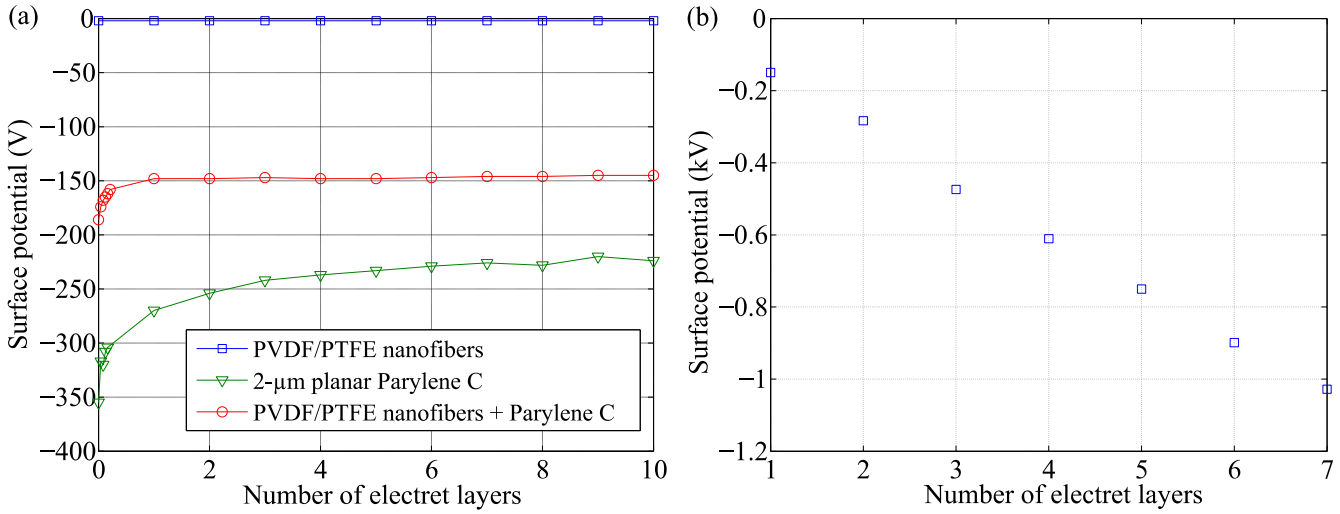

Figure 5. (a) Surface potential evolution of single-layer nanofabrous film after corona charging with and without parylene C. (b) Initial surface potential of stacked multi-layered nanofabrous electret.

samples are heated at a constant temperature of 90 °C during the 30 min of the entire charging procedure. The charged materials include a Parylene C film of 2 μm thick on top of a silicon substrate, a bare electrospun nanofibrous film without Parylene C, and an electrospun mat with the same weight of Parylene C as the planar material. The surface potential evolution with time after corona charging is recorded with a non-contact voltmeter TREK Model 347 and shown in figure 5(a).

It is observed that the bare PVDF/PTFE nanofibers can hardly preserve any charge, thus cannot be directly used as electret. In contrast, the nanofibrous film covered with Parylene C shows a higher stability of charge storage than the planar Parylene C even though its initial surface potential is 45% lower. The surface potential of PVDF/PTFE-Parylene C film stabilizes within only 1 day, faster than the planar Parylene C film (7 days). Moreover, the ratio of the remaining surface potential to initial one of PVDF/PTFE-Parylene C film is 82%, which is higher than that of 2 μm planar Parylene C film (64%). A higher proportion of charge is preserved by the nanofiber-based electret (PVDF/PTFE-Parylene C film), probably due to a larger specific surface area. The interference between the stored charges could be miniaturized, beneficial to the long-term storage of charge. However, both the initial and the remaining surface potential of the PVDF/PTFE-Parylene C film are lower than those of the planar Parylene C film, the probable cause of which is a thickness of deposited Parylene C smaller than 2 μm in the nanofiber-based electret.

The initial surface potential of a stack of electret films with varied number of films is measured, as shown in figure 5(b). Each film is first charged separately and then stacked to get the surface potential. The surface potential is linearly related to the number of stacked electret layers. This can be explained as the total electrostatic field is the summary of the field generated by each layer, considering that the surface potential of each layer are approximately identical. Biased by the stacked electret films, the equivalent internal bias of the devices V_{bias} is thus linearly proportional to the number of electret films. Consequently, we can expect an enhanced output energy per cycle by inserting an additional layer of electret due to increased V_{bias}. However, the insertion of additional electret film also gives rise to a larger minimum

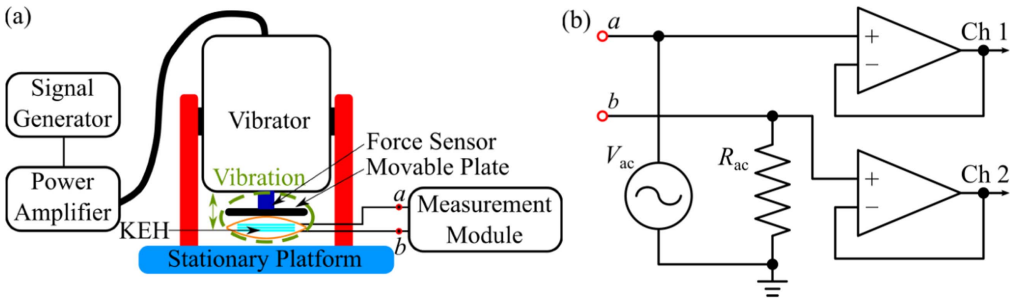

Figure 6. Experimental setup for the dynamic capacitance measurement: (a) excitation system for the proposed KEH; (b) circuit of measurement module for dynamic capacitance measurement, where nodes a and b are connected to the KEH.

gap between electrodes and consequently a smaller C_{max} while keeping an unchanged C_{min} (see section 4.1), leading to a decreased energy per cycle. Therefore, the optimal number of electret layers is determined by a tradeoff between V_{bias} and the capacitance ratio $\eta = C_{max}/C_{min}$.

4. Device performance characterization

4.1. Capacitance variation

The capacitance variation of the KEH during a vibrator-driven operation is carried out using a dynamic measurement technique introduced in [19], the experimental setup is shown in figure 6. The device is fixed on a movable plate in parallel with and at a distance from a stationary platform. The movable support is carried by a vibrator driven by a sinusoidal signal, and the device is pressed and released repeatedly through the impact and the departure between the movable support and the stationary platform. The circuit of the dynamic capacitance measurement is shown in figure 6(b): a sinusoidal AC signal V_{ac} of high frequency (named as the carrier) is applied on the KEH in series with a resistor R_{ac}. Thus the signal on node b can also be approximated as sinusoid within each period of V_{ac}. The output signals of the two followers Ch1 and Ch2 are recorded by an oscilloscope. And the variable capacitance of the KEH, C_{var}, is calculated afterwards through Matlab programming according to the following equation:

$$C_{var} = \frac{1}{2\pi f_c \tan(\theta) R_{ac}}, \tag{6}$$

where f_c stands for the frequency of the carrier, and θ is the phase difference between the output signals Ch1 and Ch2, which the calculation of each point is based on 100 periods of V_{ac} signal. The optimal load that leads to the lowest error is given by equation (7).

$$R_{ac\_opt} = \frac{1}{2\pi f_c C_{var\_m}}, \tag{7}$$

where C_{var_m} stands for the mean value of the maximum and the minimum of C_{var}.

The excitation frequency of the device is 10 Hz. Note that although this excitation frequency is quite high for wearable electronics, it is chosen considering that the capacitance variation of the device will hardly be affected by a further frequency drop. The excitation frequency is also adapted to the functions of the used oscilloscope (memory, sampling rate, etc) and the vibrator (displacement limit, drive limit, etc).

The periodic force applied on the prototype is measured by a force sensor, the amplitude of which is 0.5 N. In order to adapt to the excitation frequency, the carrier frequency has been chosen as 50 kHz, i.e., 5000 sampling points in each period of excitation movement, while the error of measurement is no more than 5 pF. And the minimum and maximum capacitances of the prototype are first measured by an impedance-meter offering an initial reference for choosing the optimal resistance for measurement. The parasitic capacitance of measurement setup (28 pF) is subtracted from the total measured capacitance [18].

The transient capacitance variation during one excitation period is shown in figure 7(a), where each curve describes the behavior of one electret configuration. The common behavior of devices is observed: the capacitance of the device when there is no impact stays at the lowest value of ~25 pF. In addition, there are two separate pulses of capacitance variation in a row during each period of vibration, the amplitude of which (C_{max1}, C_{max2} respectively) are located in the areas circled by the dash lines. The first pulse is induced by the impact between the vibrator and the fixed stopper. Its time span is short (~5 ms) due to the short duration of the impact on the springless structure. Even though the velocity of the vibrator is inversed by the impact, it will shortly be inversed again by the continuous internal force of the vibrator, resulting in a second impact. Consequently a second pulse of capacitance variation is formed. However, the velocity before the second impact is smaller than the first one, and the peak capacitance of the second pulse C_{max2} is about 10 pF lower than C_{max1}, while the time span of the second pulse is 6 times larger (~30 ms) than the first pulse.

Shown in figure 7(b) are the two featured peak values of capacitance (C_{max1} and C_{max2}) and the minimum capacitance C_{min} of the prototype in relation with the number of electret layers. C_{min} is calculated by taking the average value of C_{var} in the period without pulses, so that the error introduced by the measurement can be minimized. According to figure 7(b), C_{min} is hardly influenced by the number of the electret layers as expected, due to the non-changing maximum gap between electrodes predefined by the mechanical support structure, i.e., the insulating tape connecting the two electrodes. In contrast, both C_{max1} and C_{max2} decrease with an increased

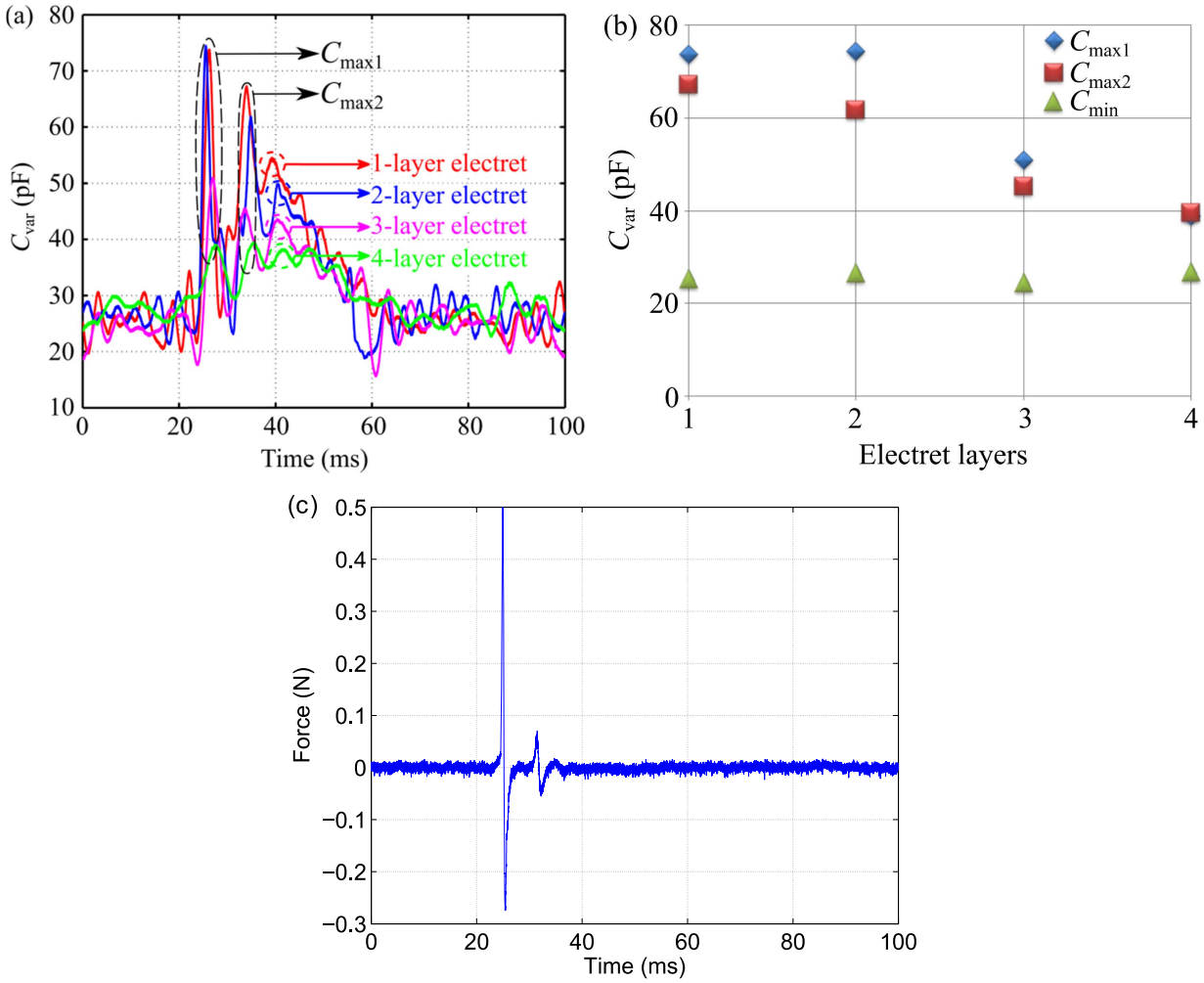

Figure 7. (a) Capacitance variation of the prototype with varied number of stacked electret films when excited by 10 Hz pressing-releasing operation (the peak force is ∼0.5 N). (b) C_{max} corresponding to the peak of two capacitance pulses (C_{max1} and C_{max2}) induced by the 10 Hz pressing movement and C_{min} of prototypes with varied number of stacked electret layers. The parasitic capacitance of 28 pF is subtracted from the total measured capacitance. (c) The force variation in one period of mechanical excitation with 3-layer electret configuration.

number of electret layers, because they are both related to the total thickness of stacked electret films.

For the configurations with 1–3 layers of electret, although the amplitude of the second impact force is only ∼1/10 of the first one. A time-dependent force variation is given by the force sensor as shown in figure 7(c), in which case the KEH contains 3 electret layers. The peak amplitude of capacitance is only reduced by less than 20%. This phenomenon indicates that the device deformation driven by the pressing force is divided into two regimes. In the first regime, the deformation occurs majorly to the supporting mechanical structures of the device including the paper substrate and the insulating tape. In the second regime, the pressure further deforms the electret layers. The force needed by the first regime is far smaller than the second regime, but the gap decrease between electrodes in the first regime is more significant. Moreover, with the configuration of 4 electret films, the two capacitance pulses have the same amplitude. This indicates that the force of 0.5 N is not sufficient to drive the deformation into the second regime for this configuration.

The bouncing behavior described above only exists in the operations with vibrators, but not shared by the case with finger-tapping. In the finger-tapping operation, the capacitance variation only reaches one peak within one tap, i.e., the finger gets away from the harvester after only one impact on the electrode. This behavior can be affirmed by the transient output voltage shown in section 4.2.

4.2. Power delivery with resistive loads

The transient output of the device working with just a resistive load and with different electret configurations (varied number of stacked electret layers) are tested with manual operations. In order to find the best conditions, the values of the resistive loads are varied from 1 to 100 MΩ, as shown in figure 8. Both the peak voltage and the peak power are plotted in relation to the load resistance, while the power with varied electret configurations is shown as different curves. The inset plotting of figure 8(a) shows the transient voltage signal on the optimal resistive load of 16 MΩ which is featured with narrow peaks having high amplitudes and small timespans.

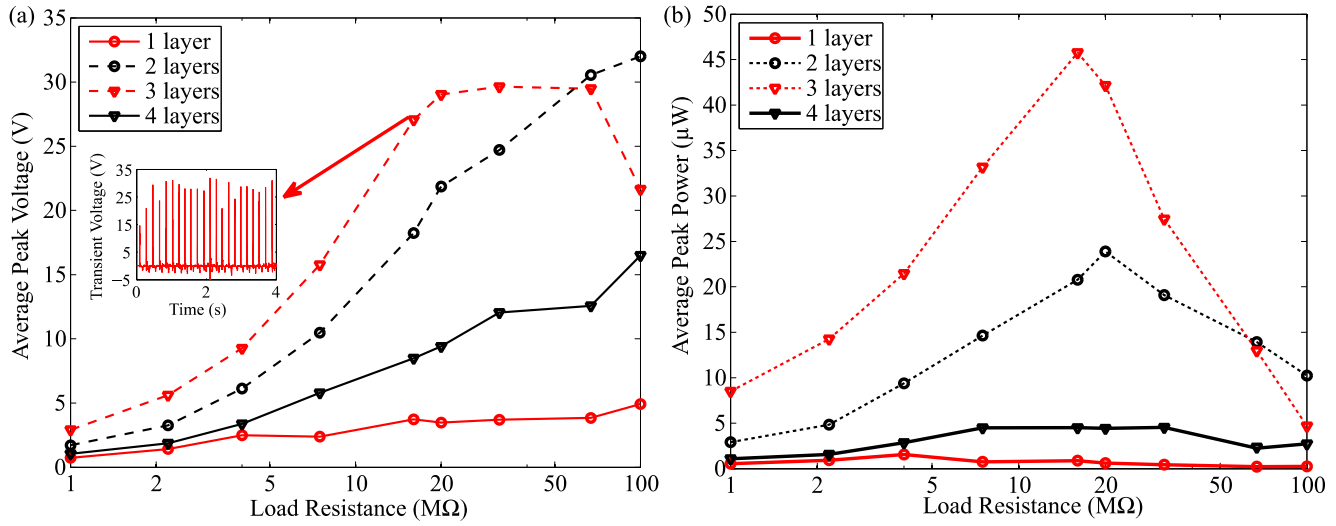

Figure 8. (a) Average peak voltage and (b) power with sweeping load. The inset plot in (a) is the transient output voltage when the device is working with the optimal configuration.

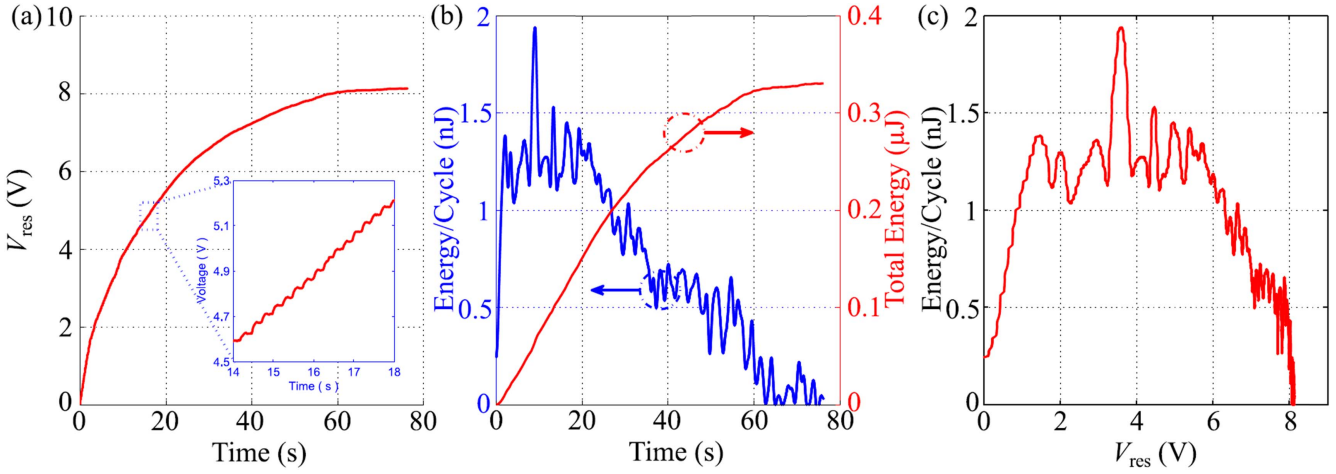

Figure 9. Finger-tap (manual operation) charging of a capacitor $C_{res} = 10$ nF through a full-wave rectifier with the tapping frequency of ~4 Hz: (a) evolution of V_{res} with time, (b) the energy per cycle and the total energy versus the time, (c) the energy per cycle versus the voltage.

The peak values vary from one pulse to another, which is induced by the inaccuracy of manual operation. The average peak voltage is calculated for each load resistance according to the transient signals so that the error brought by manual operation can be minimized, and the average peak power is calculated accordingly.

As stated in the previous section, the performances of the prototype are affected by the number of electret layers in two senses: increasing a layer of electret in the prototype leads to a growth of V_{bias}, and also results in a larger minimum gap and consequently a smaller C_{max} and smaller ratio η. Thus, the optimal electret configuration is reached through a trade-off between these two effects, maximizing the output power. According to the measurements, the maximum peak power is achieved with a 3-layer electret, while the optimal resistive load is 16 MΩ. The average width of the pulses in the transient signals is ~30 ms. Under this optimal configuration, the peak output voltage is 27 V; the peak instantaneous output power is 45.6 μW (the average power is 0.29 μW), and the average energy per tap is 53 nJ.

4.3. Power delivery with a full-wave diode bridge

In order to evaluate the DC power delivery capability of the best prototype, the device is tested in cooperation with a full-wave diode bridge rectifying circuit. In the first experiment, the KEH is driven manually (under the same excitation conditions as in section 4.2) and works in cooperation with a full-wave rectifier, the results are shown in figure 9. A reservoir capacitor $C_{res} = 10$ nF is charged up to 8.2 V within 210 finger taps on the device with a frequency of ~4 Hz. The evolution of V_{res}, the voltage accross C_{res}, is shown in figure 9(a).

Shown in figure 9(b) is the evolution of the energy conserved in C_{res} per cycle of excitation and the total energy in C_{res}. The energy converted within each charging cycle can be calculated accordingly. The total energy accumulated

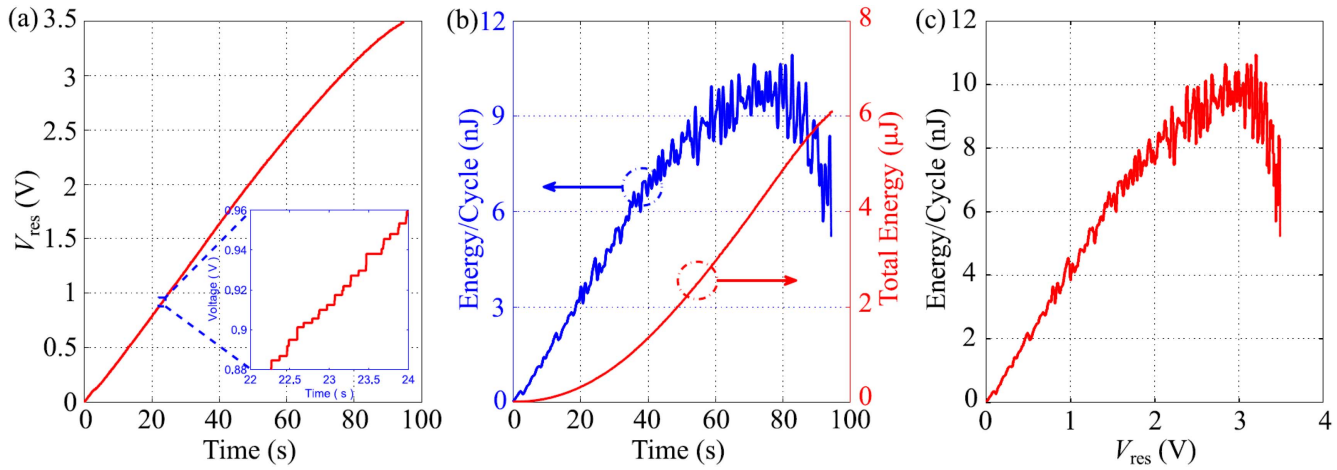

Figure 10. Shaker-driven charging of a capacitor $C_{res} = 1\ \mu$F through a full-wave rectifier with the tapping frequency of 10 Hz with the peak force of 0.5 N: (a) evolution of V_{res} with time, (b) the energy per cycle and the total energy versus the time, (c) the energy per cycle versus the voltage.

during the entire charging process is 0.34 μJ (210 taps in total), corresponding to an average energy of 1.6 nJ/tap. While the maximum energy delivery is reached when V_{res} is about 3.5 V and is equal to 1.95 nJ/cycle, corresponding to an optimal power of 11.7 nW (figure 8(c)) This power is far less than that with the optimal resistive load (the average power 0.29 μW and the peak instantaneous power of 45.6 μW as stated in section 4.2). It results from two effects: the impedance mismatch effect between the rectifying circuit and the optimal resistive load; and the voltage drop of diodes filtering the signals with small amplitude.

In the second experiment, the device is pressed with a repetitive and controllable motion provided by a vibrator, so that the power delivery of the KEH in cooperation with an AC–DC rectifying circuit can be characterized in a stable frequency and uniform force. The schematic of the excitation system for the KEH is shown in figure 6(a). The storage capacitance of the device is 1 μF so that the energy released from the capacitor discharging from 3.3 V down to 1.1 V is able to sustain up to 3 RFID communications, each communication consuming 1.77 μJ of energy [20]. The excitation signal applied on the vibrator is set at 10 Hz, while the maximum force applied is 0.5 N. The rectifying circuit tested is a full-wave diode rectifier. The evolution of V_{res} versus time is shown in figure 10(a). Figure 10(b) shows the time-dependent total energy stored in the capacitor, together with the energy transferred to the capacitor during each cycle of charging. It is inferred that the duration of the entire charging process from 0 to 3.3 V is 87 s, and the accumulated energy is 5.5 μJ, corresponding to an average power of 63 nW. Considering the operation frequency of 10 Hz, the average energy accumulated during each cycle is 6.3 nJ. While the recharging process from 1.1 V back to 3.3 V takes 59 s, during which the average power is 82 nW or the energy of 8.2 nJ/cycle.

From figure 10(c) it can be observed that the energy accumulated during each cycle is approximately linear within the range of low storage voltage below 2 V. Within this stage, the charge pumped into the storage capacitor within each tapping operation is almost constant, about 4 nC/cycle. This indicates that the internal bias is capable of pumping a constant amount of charge to the capacitor during each cycle regardless of the increase of the barrier voltage, the sum of the voltage on the storage capacitor V_{res} and the forward voltage drop of the diodes. However, when V_{res} further increase, some of the charges flowing between the two electrodes are blocked from traveling due to a higher barrier voltage, resulting in a smaller amount of delivered charge Q. Since the energy stored to the capacitor is proportional to both V_{res} and Q, the increasing V_{res} accompanied by the decrease of Q, the increase of energy delivered per tap firstly reaches a maximum value and finally drops. Thus there is an optimal V_{res} corresponding to the maximum energy delivery to the storage capacitor per cycle. According to the graph, a maximum power of 99 nW (energy of 9.9 nJ/cycle) is reached when V_{res}, is 3 V, while the power is no less than 80 nW (energy of 8 nJ/cycle) when V_{res} is between 2 and 3.3 V.

5. Conclusion

In this paper, we have introduced the first flexible electret KEH. It is based on a low-cost sandwich-structure implementing stacked nanofiber-based electret films. Thanks to its thin-film components, the design is light-weighted and is less than 1 mm in thickness when it is pressed, thus suitable for wearable electronics. Although as-electrospun nanofibrous material is not suitable for working directly as electret, we propose to cover it with a parylene C layer in order to offer a stable charge storage. However, since the Paryelene C on the electrospun nanofibers has a smaller thickness compared to the planar Parylene C film, its long-term surface potential is lower, and needs to be further improved to take full advantage of its large specific area. The best energy conversion is obtained with a ratio of capacitance variation of 5 with a 3-layer electret. The optimal resistive load of the prototype is 16 MΩ, while the maximum peak power obtained is 45.6 μW, corresponding to 48 nJ/cycle. The typical energy conversion density of piezoelectric KEHs is 0.1–1 μJ cm^{-2} per cycle

[5, 6], while triboelectric KEHs typically offer peak instantaneous power of $\sim 10\,\mu W\,cm^{-2}$ [3]. In comparison, the current prototype has an energy density of 8 $nJ\,cm^{-2}$/cycle. The prototype is able to deliver an optimal energy of 9.9 nJ/cycle with a regular tapping of 0.5 N when working with full-wave conditioning circuit. The optimal energy delivery is relevant to the DC voltage on the storage capacitor and the two key parameters of the prototype, the internal bias voltage and the ratio of capacitance variation. In a finger-tapping experiment, the device charges a capacitor of 10 nF up to 8.5 V within 450 strokes through a full-wave rectifier. The power transmission can be improved through a better impedance matching or a reduced diode voltage drop.

ORCID iDs

Y Lu https://orcid.org/0000-0003-0726-5653
Y Leprince-Wang https://orcid.org/0000-0002-9876-3852
P Basset https://orcid.org/0000-0002-9790-8247

References

[1] Hwang G, Byun M, Jeong C K and Lee K J 2015 Flexible piezoelectric thin-film energy harvesters and nanosensors for biomedical applications *Adv. Helthcare Mater.* **4** 646–58
[2] Kachroudi A, Basrour S, Rufer L, Sylvestre A and Jomni F 2016 Micro-structured PDMS piezoelectric enhancement through charging conditions *Smart Mater. Struct.* **25** 105027
[3] Bai P, Zhu G, Lin Z H, Jing Q, Chen J, Zhang G, Ma J and Wang Z L 2013 Integrated multilayered triboelectric nanogenerator for harvesting biomechanical energy from human motions *ACS Nano* **7** 3713–9
[4] Meng B, Tang W, Zhang X, Han M, Liu W and Zhang H 2013 Self-powered flexible printed circuit board with integrated triboelectric generator *Nano Energy* **2** 1101–6
[5] Almusallam A, Luo Z, Komolafe A, Yang K, Robinson A, Torah R and Beeby S 2017 Flexible piezoelectric nano-composite films for kinetic energy harvesting from textiles *Nano Energy* **33** 146–56
[6] Delnavaz A and Voix J 2014 Flexible piezoelectric energy harvesting from jaw movements *Smart Mater. Struct.* **23** 105020
[7] Meninger S, Mur-Miranda J O, Amirtharajah R, Chandrakasan A and Lang J H 2001 Vibration-to-electric energy conversion *IEEE Trans. Very Large Scale Integr. (VLSI) Syst.* **9** 64–76
[8] Sakane Y, Suzuki Y and Kasagi N 2008 The development of a high-performance perfluorinated polymer electret and its application to micro power generation *J. Micromech. Microeng.* **18** 104011
[9] Collins R E 1975 Distribution of charge in electrets *Appl. Phys. Lett.* **26** 675–7
[10] Mishra A 1982 Studies of polymer electrets: II. Factors governing the stabilities of homoelectrets obtained from polystyrene and its derivatives *J. Appl. Polym. Sci.* **27** 1107–18
[11] Budinger W D 1995 *US Patent No.* 5,384,337Washington, DC: U.S. Patent and Trademark Office
[12] Kashiwagi K, Okano K, Miyajima T, Sera Y, Tanabe N, Morizawa Y and Suzuki Y 2011 Nano-cluster-enhanced high-performance perfluoro-polymer electrets for energy harvesting *J. Micromech. Microeng.* **21** 125016
[13] Lo H W and Tai Y C 2008 Parylene-based electret power generators *J. Micromech. Microeng.* **18** 104006
[14] Li D and Xia Y 2004 Electrospinning of nanofibers: reinventing the wheel? *Adv. Mater.* **16** 1151–70
[15] Greiner A and Wendorff J H 2007 Electrospinning: a fascinating method for the preparation of ultrathin fibers *Angew. Chem. Int. Ed.* **46** 5670–703
[16] Ignatova M, Yovcheva T, Viraneva A, Mekishev G, Manolova N and Rashkov I 2008 Study of charge storage in the nanofibrous poly (ethylene terephthalate) electrets prepared by electrospinning or by corona discharge method *Eur. Polym. J.* **44** 1962–7
[17] Basset P, Blokhina E and Galayko D 2016 *Electrostatic Kinetic Energy Harvesting* (New York: Wiley)
[18] Lu Y, O'Riordan E, Cottone F, Boisseau S, Galayko D, Blokhina E, Marty F and Basset P 2016 A batch-fabricated electret-biased wideband MEMS vibration energy harvester with frequency-up conversion behavior powering a UHF wireless sensor node *J. Micromech. Microeng.* **26** 124004
[19] Basset P, Galayko D, Paracha A M, Marty F, Dudka A and Bourouina T 2009 A batch-fabricated and electret-free silicon electrostatic vibration energy harvester *J. Micromech. Microeng.* **19** 115025
[20] Lu Y, Basset P and Laheurte J-M 2017 Performance evaluation of a long-range RFID tag powered by a vibration energy harvester *IEEE Ant. Wirel. Prop. Lett.* **16** 1832–5